Desalination and Water Treatment
www.deswater.com
doi: 10.5004/dwt.2020.24961

178 (2020) 143–154
February

Ammonia removal from aqueous solution by sodium functionalized graphene oxide: isotherm, kinetics, and thermodynamics

Arghavan Mirahsani[a], Javier B. Giorgi[b,*], Majid Sartaj[a]

[a]*Department of Civil Engineering, University of Ottawa, 161 Louis Pasteur, Ottawa, ON, K1N 6N5, Canada, Tel. +1(613)715-1367; email: amira067@uottawa.ca, Tel. +1(613)612-6622; email: msartaj@uottawa.ca*
[b]*Department of Chemistry and Biomolecular Sciences, University of Ottawa, 10 Marie Curie Private, Ottawa, ON, K1N 6N5, Canada, Tel. +1(613)562-5800 Ext: 6037; email: Javier.Giorgi@uottawa.ca*

Received 20 March 2019; Accepted 22 September 2019

ABSTRACT

Municipal, industrial, and agricultural wastewaters contain high concentrations of nitrogen in the form of ammonia and ammonium ions. This nitrogen has a range of polluting effects and must be removed before discharge. Multiple methods are currently under investigation for the removal or capture of total ammonia nitrogen (TAN). TAN in aqueous media shows unique behavior making it necessary to study its interactions with potential absorbents in detail. In this study, sodium functionalized graphene oxide (GO-Na) was used for TAN removal from aqueous media by ion exchange. Batch adsorption experiments were performed to investigate the adsorption capacity of GO-Na and. The mechanism of adsorption was investigated using multiple models including Elovich and intra-particle diffusion models. The adsorption kinetics followed the pseudo-second-order model. Experimental data was well described by a Langmuir isotherm model with a maximum adsorption capacity of 32 mg/g. The adsorption energies and thermodynamic parameters indicated weak interactions were dominant with an overall exothermic and spontaneous process. The weak interactions resulted from the ion-exchange of sodium cation on the surface of graphene oxide with ammonium cations in the liquid phase, which also results in the easy regeneration of the adsorbent with NaCl which is a non-toxic, environmentally friendly and inexpensive salt in nature.

Keywords: Graphene oxide; Ammonia; Adsorption; TAN removal; Isotherm; Kinetic; Thermodynamic

1. Introduction

Ammonia (NH_3) is the most abundant nitrogen-containing pollutant in the environment. It enters water resources through industrial, municipal, and agricultural discharges yearly. In aquatic chemistry, ammonia can be found in the form of ammonium cations (NH_4^+) and molecular ammonia (NH_3); the sum of these two forms is expressed as total ammonia nitrogen (TAN). The range and average of TAN in municipal wastewaters is reported to be 12–50 mg/L and 30 mg N/L, respectively [1]. The major environmental concerns of ammonia include eutrophication [2], depletion of dissolved oxygen in water resources [3], and toxicity to fish and other aquatic species even at a concentration as NH_3 low as 0.2 mg/L [4]. Also, TAN has several harmful effects on the human skin, eyes, and respiratory system [5,6].

With the rapid growth of environmental awareness over the past century, many environmental standard limits were set to control the release of ammonia into the water bodies. Total ammonia nitrogen (TAN) toxicity is mainly related to dissolved ammonia in water bodies and the distribution of dissolved ammonia to ammonium cation is a function of two important factors; pH and temperature [7]. US EPA has set two standard limits as acute and chronic limits to protect the aquatic life based on pH and temperature. At pH of

* Corresponding author.

7 and temperature of 20°C, the US EPA acute criterion and the chronic levels are 17 and 1.9 mg TAN/L, respectively [4]. Methods proposed for TAN removal from wastewater include the biological nitrification–denitrification process [8], air stripping [9], chemical precipitation [10], ultra-sonication and microwave [11], ion exchange and adsorption [12–22]. Among these techniques, adsorption is the most frequently used technology due to its simple and economical operation, less sludge production resulting in fewer disposal problems, and the potential for recovery of ammonium cations [23,24]. The most widely used adsorbents and/or ion exchangers are zeolites [12–22], mesoporous silica materials [25,26], and resins [27,28]. Rat-Valdambrini et al. [26] investigated the application of arene-sulfonic acid functionalized SBA-15 on ammonium cation removal from an aquatic solution. They reported the maximum adsorption capacity can be reached at 5°C and it was estimated around 19 mg NH_4^+/g of adsorbent. Ding and Sartaj [29] also optimized the operational conditions for TAN removal by zeolite and resin [27] and compared the performances of these two ion exchangers. They claimed the optimum TAN uptake by a natural zeolite was estimated as 22.9 mg/g [29], while for resins it was reported as 28.78 mg/g [30].

In the last decade, the appearance of graphene has provided researchers a newly emerging family of materials for contaminant removal from aquatic solutions by incorporation of these new materials into a variety of technologies [31]. Graphene is defined as one atomic layer of graphite in which a layer of carbon atoms bonded together in a hexagonal or honeycomb lattice [32] provides a light, highly functionalizable material with an extremely high surface area. Perhaps the easiest and more versatile way to functionalize graphene is by oxidation, where oxygen-containing functional groups such as hydroxyl, carboxyl, and epoxy groups can be added to form graphene oxide (GO).

Previous studies reported on the performance of graphene-based material for removing various wastewater contaminants such as dyes [33–37], pharmaceuticals [38,39], and heavy metals [40–44]. In addition, recently many studies have investigated the application of graphene-based materials for ammonia gas adsorption [45–48]. However, the adsorption capacity of graphene-based materials for TAN removal in aquatic media has not been previously reported. TAN in aqueous media shows unique binding and equilibrium behavior making it necessary to study its interactions with the absorbent in detail. In this study, GO was synthesized and further sodium functionalized graphene oxide (GO-Na), and its capacity in adsorption of TAN from aqueous solution was investigated. The produced material was characterized and a full kinetic, isotherm and thermodynamic study was performed to reach a better understanding of the adsorption behavior of TAN on GO-Na.

2. Experimental setup

2.1. Chemicals and materials

Synthetic graphite powder, –20 + 80 mesh, 99.9% (metals basis) was obtained from Alfa Aesar (USA). Sulfuric acid (98%) and potassium permanganate were purchased from Anachemia (Canada). Phosphoric acid (85%) and hydrogen peroxide (30%) were purchased from Fisher Scientific (Cananda). Ammonia TNTplus Vials (HR 2–47 mg/L NH_3–N) were purchased from HACH (Canada).

2.2. GO synthesis by improved Hummer's method

GO was prepared according to an improved Hummer's method at room temperature (24°C) [49]. In a beaker, 360 mL of H_2SO_4, 40 ml of H_3PO_4, 37 g of $KMnO_4$, and 7 g of graphite powder were mixed and remained under stirring for a week at room temperature. Due to the exothermicity of the reaction, the temperature of the suspension initially increased to 40°C and then slowly dropped back to room temperature. During this step, the color of the suspension was initially purplish green and gradually turned to dark brown. After a week, the suspension became light brown, indicating that a high oxidation level had been achieved. Then, 2 L of de-ionized (DI) water and 80 mL of H_2O_2 30% were added to the mixture to end the oxidation process. For safety and to control the temperature, water was added drop by drop and gently. The resulting solution was centrifuged at 12,000 rpm for 15 min. Upon removal of the supernatant, the material was treated with 400 mL of HCl (1 M) and put under stirring for 2 h to remove all impurities. The mixture was centrifuged again at 12,000 rpm and the brown deposit was washed with DI water under filtration until the pH of the solution reached 4. The resulting washed material is hereby labeled as GO.

2.3. Sodium functionalized graphene oxide

1.5 g of GO was added to 150 mL of NaOH (1 M) at 40°C and put under stirring for 30 min until the brownish GO completely turned to black. The suspension was centrifuged at 12,000 rpm and then mixed with 250 mL of NaCl (10% w) at room temperature and stirred for another 30 min to fully saturate all active sites with sodium. Finally, the mixture was centrifuged and washed with DI water until pH 9 was obtained. The resulting material was dried at room temperature and labeled GO-Na.

2.4. Material characterization

Samples were characterized during the preparation process (GO and GO-Na) as well as after adsorption (GO-Na-N). Morphological structures of samples were examined by transmission electron microscopy (TEM) with a Tecnai Spirit TEM instrument. The Fourier transform infrared (FTIR) spectra were collected on a Nicolet 6700 FTIR spectrometer using an attenuated total reflection accessory. The spectra were recorded for suspended material in aqueous solution from 4,000 to 400 cm^{-1} (128 co-added scans). Raman spectroscopy of three samples was collected with a Thermo Scientific Raman microscope (USA). X-ray photoelectron spectroscopy (XPS) measurements were obtained on a Kratos AXIS Ultra DLD 39-3061 (UK) using a monochromated Al source.

2.5. Adsorption studies

A stock solution of NH_4Cl was used to study the adsorption properties of TAN by GO-Na. Batch-adsorption

experiments were performed in 100 mL beakers magnetically stirred. The adsorption isotherms were obtained using NH_4Cl solutions with initial concentrations of 10–100 mg/L and adsorbent dosage of 1 g/L, with each test, replicated 3 times. A kinetic analysis was performed with intermediate TAN concentration (50 mg/L) and an adsorbent loading of 1 g/L, measuring TAN uptake as a function of time for 20 min at different time intervals. A thermodynamic investigation was performed by conducting adsorption tests with intermediate TAN concentration (50 mg/L) and adsorbent dosage of 1 g/L, under three different temperatures (7°C, 24°C, and 42°C), results of which were used to calculate enthalpy and entropy parameters. The pH of all batch adsorption experiments was around neutral in which ammonia nitrogen is mostly in the form of ammonium cations. In all cases, after the adsorption experiments, all the solutions were filtered through a polytetrafluoroethylene (PTFE) membrane filter (0.2 micron) over the vacuum.

TAN concentration was measured using HACH ammonia TNTplus Vials (HR 2–47 mg/L NH_3–N) and a DR6000TM UV-VIS HACH Spectrophotometer with RFID technology according to the salicylate method (Method: 10205). The removal percentage (R%) and solid phase concentration (q_e in mg/g) were calculated as follows:

$$R\% = \left(\frac{C_0 - C_e}{C_0}\right) \times 100 \quad (1)$$

$$q_e = \left(\frac{C_0 - C_e}{W}\right) \times V \quad (2)$$

where C_0 and C_e (mg/L) are the initial and equilibrium concentration of TAN in solution, respectively, W (g) is the mass of adsorbent, and V (L) is the volume of solution.

To study the regeneration capacity, the used adsorbent for the kinetic part was added to sodium chloride solution (10% w) and remained under stirring for 4 h. Then, it was washed with DI water over the vacuum filter. Finally, it was dried at room temperature and used for a subsequent cycle of adsorption tests with an adsorbent dose of 1 g/L, the initial TAN concentration of 50 mg/L, around neutral pH.

3. Results and discussion

3.1. Adsorbent characterization

The nature of the adsorbent was determined using typical characterization features for GO as reference. Fig. 1 shows the Raman spectra for the synthesized GO, GO-Na and the used GO-Na after adsorption (GO-Na-N). The characteristic graphite Raman spectrum is shown for comparison. The different forms of GO can be evaluated by the ratio of D to G bands in the spectra, which are related to the degree of disruption of the hexagonal network (D = defective, sp^3 or disordered carbon; G = sp^2 carbon). The as-produced GO shows a ratio of D to G bands at approximately 1 (I_D/I_G = 1.0). GO-Na shows an increase in the ratio (I_D/I_G = 1.1) emphasizing the additional disruption to the graphene network, and upon exchange with ammonium ions, the ratio remains at approximately that value.

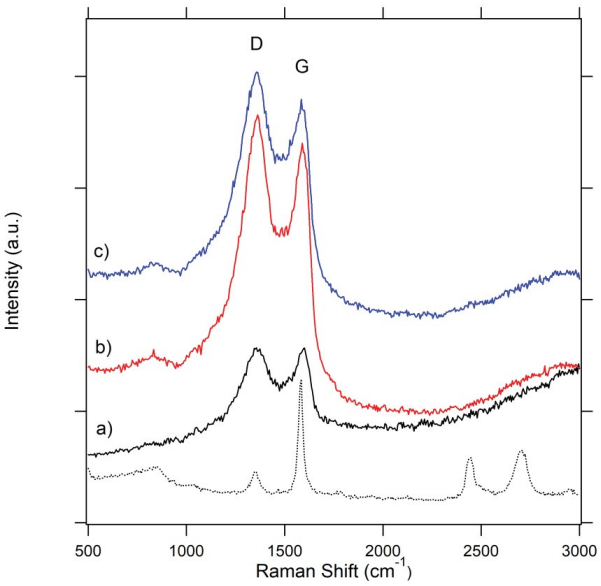

Fig. 1. Raman spectra of (a) GO, (b) GO-Na, and (c) GO-Na-N. Characteristic D and G bands of graphene have been labeled. Dotted spectrum corresponds to graphite, for reference.

The actual functional groups present in the materials were explored by infrared absorption and photoelectron spectroscopy. Fig. 2 shows the XP spectra for the three materials. Besides the expected carbon and oxygen peaks, GO contains traces of nitrogen. In the case of GO-Na, the typical peaks of sodium are seen in the spectrum. Upon utilization of the GO-Na for adsorption of ammonium, the exchange can be easily identified by the reduction of the sodium peaks and the increase in the nitrogen signal.

Speciation of the functional groups using XPS was performed by considering the C 1 s spectra for the three materials. The binding energy spectrum for GO shows two sharp peaks at 283.6 and 285.8 eV, characteristic of C bound to other carbons (as in the graphene backbone) and carbon bound to oxygen via ether like groups (labeled as C–C and C–O–C in

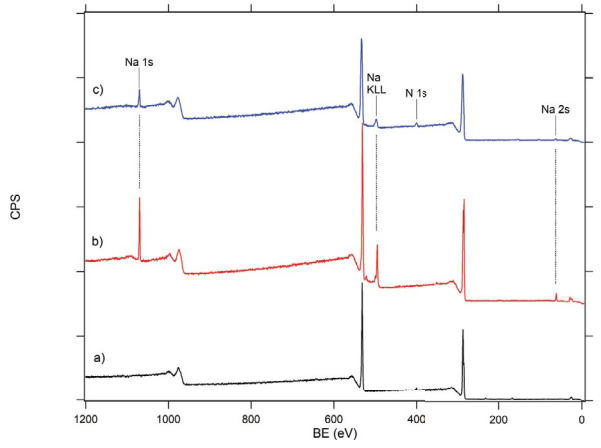

Fig. 2. XPS surveys for (a) GO, (b) GO-Na, and (c) GO-Na-N. Characteristic carbon and oxygen peaks around 285 and 532 eV are not labeled.

Fig. 3). In addition, a broad high binding energy peak can be seen which includes the contributions of multiple other oxygen bound carbon species (acid, alcohol, and carbonyl). While fitting the spectrum to obtain quantitative identification of potential carbon functional groups is possible, the width of the observed peak prevents an unbiased identification. Thus, considering the qualitative trend is more suitable to understand the characteristics of the material at each step. Upon treatment with NaOH, a reduction of the GO can be observed by the increase in the C 1s peak at 283.6 eV (increase in C–C) and a decrease in the highly oxygenated species at higher binding energy. It is unclear how the sodium interacts with the carbon framework. Interestingly, the adsorption of TAN shows an increase in the high binding energy peaks as well as a broadening of peaks corresponding to all the species. This is consistent with the appearance of new nitrogen-containing carbon species such as amide groups.

The presence of the C–O–C species as dominant in the GO materials was corroborated by FTIR (Fig. 4). The GO spectrum contains the characteristic peaks at 1,750; 1,616; 1,214; and 972 cm^{-1} (with a shoulder at 1,050 cm^{-1}). These peaks correspond to the C=O (in –COOH), C=C bend, phenolic C–O and epoxy CO, respectively [50–52]. The OH region is broad, likely due to ambient water, but a shoulder is also observed at the characteristic 3,400 cm^{-1} for alcohol groups in GO. Upon NaOH treatment, the main change is the disappearance of the peak at 1,750 cm^{-1} and a slight shift in the peak at 1,616 cm^{-1} consistent with a partial reduction of the material. The GO structure remains, but changes in the shape of the background are also observed. Adsorption of ammonium ions produces a broadening and decrease in intensity of all peaks, and the appearance of the pairing at 1,577 cm^{-1} with a shoulder at 1,660 cm^{-1} which can be attributed to the presence of N–H and C=O in amide groups [50].

The overall morphology of the GO materials was observed via electron microscopy (TEM). Fig. 5 shows the characteristic large, thin sheets of GO, which upon treatment with sodium shows folding and aggregation. The material after adsorption (GO-Na-N) appears highly aggregated consistently with the chemical changes. This might be a reason for the slight decrease in adsorption performance upon regeneration of the GO-Na, as discussed in section 3.6.

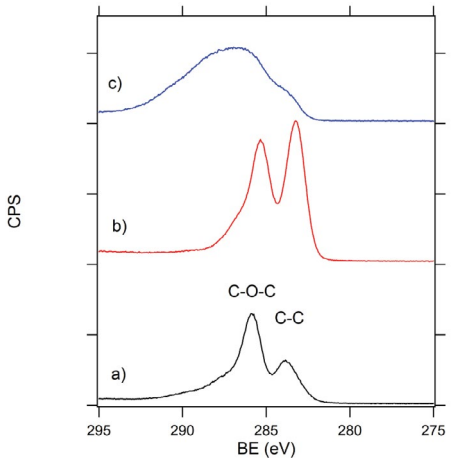

Fig. 3. C 1s XPS region for (a) GO, (b) GO-Na, and (c) GO-Na-N.

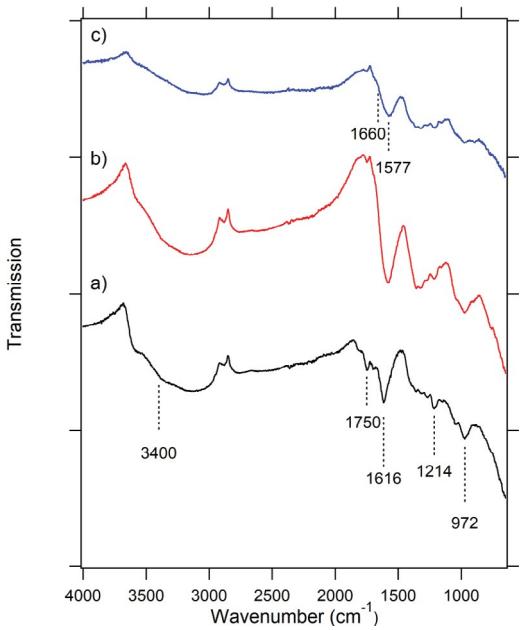

Fig. 4. FTIR spectra for (a) GO, (b) GO-Na, and (c) GO-Na-N. Characteristic peaks have been labeled. Spectra are offset for clarity.

3.2. Adsorption isotherm

To study TAN adsorption patterns in the liquid/solid phase at equilibrium conditions, adsorption isotherm tests were carried out under different initial concentrations. The adsorption isotherm was fitted according to five common isotherm models, Langmuir, Freundlich, Sips, Redlich–Peterson, and Langmuir-Freundlich (Table 1). The isotherm equations are defined below [26,53]:

Langmuir equation:

$$q_e = \frac{K_{ad} q_{Max} C_e}{1 + K_{ad} C_e} \tag{3}$$

Freundlich equation:

$$q_e = K_F C_e^{\frac{1}{n}} \tag{4}$$

Sips equation:

$$q_e = \frac{q_{Max} \left(K_{ad} C_e\right)^n}{1 + \left(K_{ad} C_e\right)^n} \tag{5}$$

Redlich–Peterson equation:

$$q_e = \frac{a C_e}{1 + K_{ad} C_e^n} \tag{6}$$

Langmuir-Freundlich equation:

$$q_e = \frac{K_{ad} q_{Max} C_e^{\frac{1}{n}}}{1 + K_{ad} C_e^{\frac{1}{n}}} \tag{7}$$

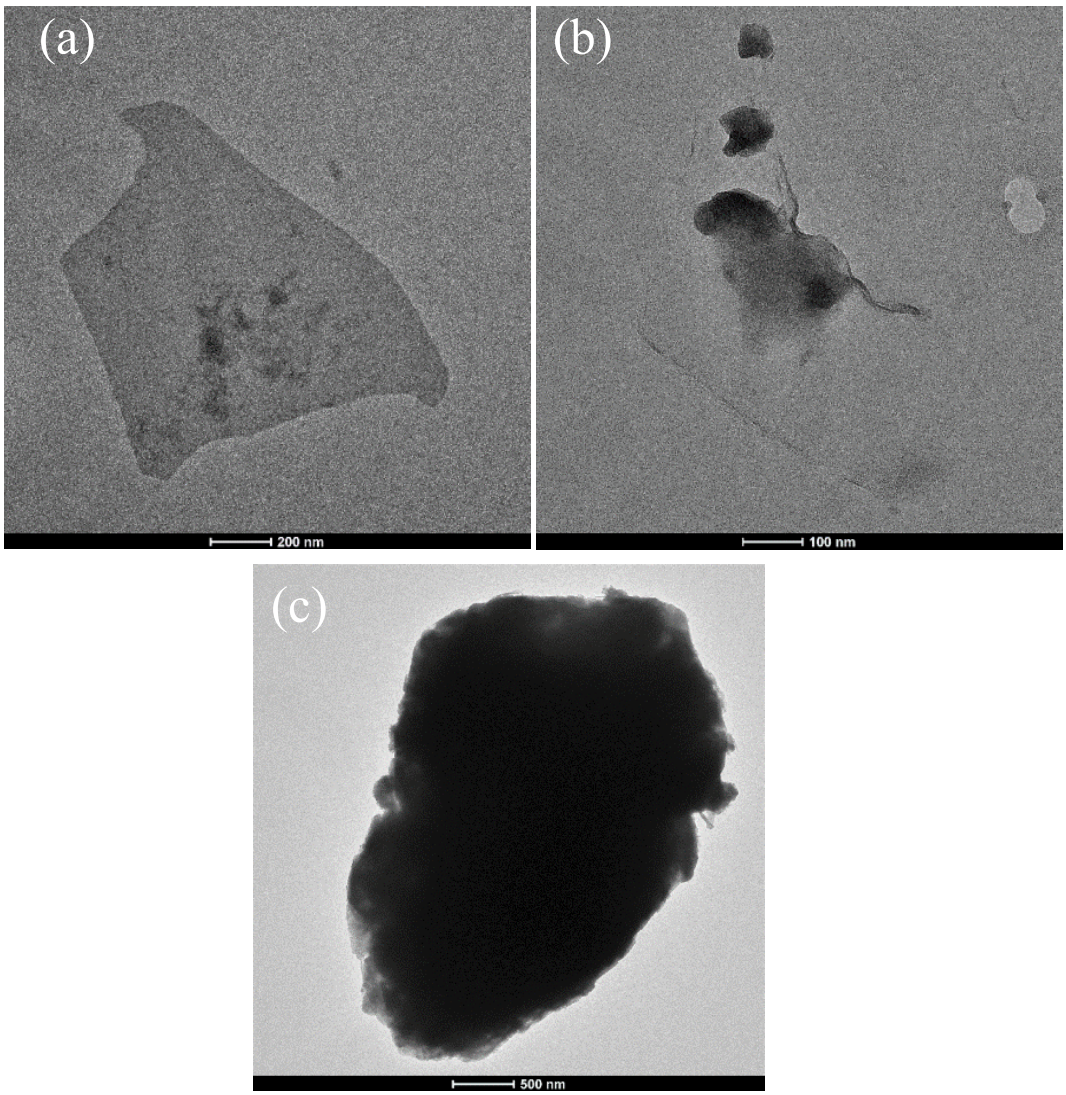

Fig. 5. TEM images for (a) GO, (b) GO-Na, and (c) GO-Na-N.

Table 1
Isotherm constants and regression correlations

Isotherm model	q_{max} (mg/g)	K_{ad} or K_F	n	a	R^2
Langmuir	32	0.09	–	–	0.99
Freundlich	–	4.73	2.29	–	0.98
Sips	40	0.04	0.74	–	0.99
Redlich–Peterson	–	4.26	0.81	0.31	0.99
Langmuir-Freundlich	33.6	0.09	1.12	–	0.99

where q_e (mg/g) is the equilibrium solid phase concentration of GO-Na; K_{ad} (L/mg) is the adsorption equilibrium constant related to the affinity of the binding site and energy of adsorption; q_{max} (mg/g) is the maximum adsorption capacity in Langmuir model; C_e (mg/L) is the equilibrium TAN concentration; K_F (mg$^{(n-1)/n}$/g L) is the Freundlich adsorption constants related to adsorption capacity; n is a constant related to surface heterogeneity, and a is the constant in the Redlich–Peterson equation ($a = K_{ad}\, q_{max}$) [53].

The two most common and contrasting isotherms (Langmuir and Freundlich) are plotted in Fig. 6. The Langmuir adsorption isotherm is the most prevalent model for recognizing the behavioral pattern of particles adsorbed on the surface of nano adsorbents in the liquid phase. This model applies to monolayer and homogeneous adsorption. This implies that all molecules have fixed positions in the adsorbent's structure and just one layer participates in the adsorption process (monolayer) [28]. Additionally, in this model, there is no interaction between molecules adsorbed on adjacent sites. The maximum adsorbent capacity reaches a saturation point under equilibrium conditions where no more adsorption can occur [54]. An alternative widely used empirical equation to describe experimental adsorption data is the Freundlich isotherm model. This model is based on multilayer and heterogeneous adsorption with interaction between adsorbed molecules [55]. According to this isotherm,

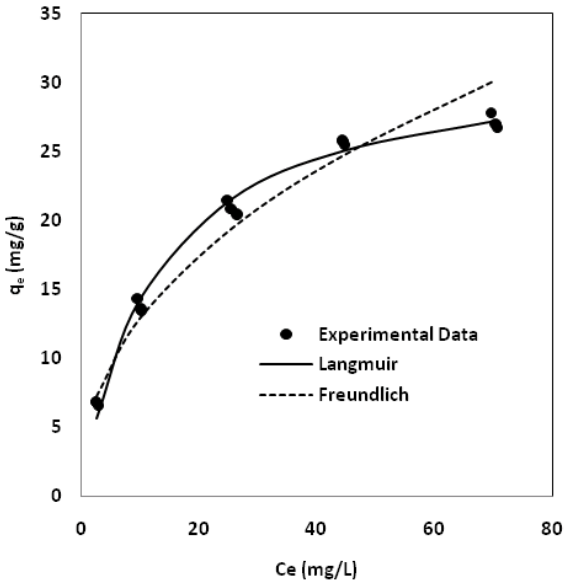

Fig. 6. Empirical and theoretical TAN adsorption isotherms on GO-Na Conditions: at room temperature, pH = 7, and dose = 1 g GO-Na/L.

the adsorption capacity will be boosted with an increase in pollutant concentration [54].

Sips, Redlich–Peterson, and Langmuir-Freundlich isotherms can be thought of as suitable combinations of the Langmuir and Freundlich isotherms applicable under different sets of conditions. The five isotherms provide a good fit to the experimental data (Table 1). However, the Langmuir model better describes the physical behavior of TAN adsorption on GO-Na. The Langmuir isotherm implies that the adsorption process titrates fairly similar sites on the GO-Na material, and therefore a single layer of adsorbent participates in the adsorption [28,54], in accordance with the physical characteristics of GO-Na. From the fit of the TAN removal data following a monolayer adsorption process as described in the Langmuir model, the maximum capacity of GO-Na was determined to be 32 mg/g.

The maximum capacity of GO-Na calculated from the Langmuir model was compared with the maximum Langmuir capacity of various adsorbents from literature, as determined under similar conditions. TAN absorption on natural and modified zeolites vary, but typical values are $q_{max} < 20$ mg/g [21,56–58], volcanic tuff has values in the same range [59], and resins can show values of q_{max} in the high twenties [60]. These typical values emphasize the potential of GO-Na synthesized in this study, which shows a higher maximum adsorption capacity (q_{max} = 32). The comparison with activated carbon (q_{max} = 6.08) [61] is particularly significant because it indicates that the nanostructure of carbon base materials with accompanying increase in surface area requires appropriate functionalization (as in the case of GO-based materials which can be considered as functionalized single carbon sheets) to produce a significant improvement of TAN adsorption capacity.

As a corollary of the applicability of the Langmuir isotherm for the adsorption of TAN on GO-Na, the separation factor (R_L) can be further calculated according to the following equation [62–65].

$$R_L = \frac{1}{1 + K_{ad} C_0} \tag{8}$$

where K_{ad} (L/mg) is the Langmuir adsorption constant and C_0 (mg/L) is the initial TAN concentration. R_L is an indicator to estimate the favorability of a reaction. Variation of R_L between 0 to 1 means a favorable process. The R_L approaches 0 if the value of K_{ad} is extremely large which indicates an irreversible reaction. Oppositely, when K_{ad} is infinitely small, the R_L value approaches 1 which means a linear process. An R_L value greater than 1 only occurs in the case that K_{ad} appears to be negative. Because K_{ad} is obtained from fitting experimental data, this occurs when there is unfavorable adsorption or leaching of contaminants to the solution during the adsorption process [56,62,63,66]. In this study, the values of R_L for increasing TAN concentrations in solution for a fixed dose of adsorbent GO-Na were calculated. The range of R_L (0.1 to 0.55) verifies the favorable adsorption behavior of TAN on GO-Na.

3.3. Adsorption energy

The mean adsorption energy for TAN adsorption by GO-Na was first calculated according to the Dubinin–Radushkevich equation (D–R), which is commonly used in the field and allows direct comparison with the literature [64,65]. The D–R approach uses a temperature-dependent isotherm and assumes a Gaussian distribution of adsorption energies on a heterogeneous surface. The model can be described by Eq. (9)

$$\ln q_e = \ln q_{max} - \beta\varepsilon^2 \tag{9}$$

where q_{max} and q_e (mg/g) is the theoretical monolayer adsorption capacity and the solid phase concentration at equilibrium, respectively; β is the constant of the adsorption energy (mol²/J²), and ε is the Polanyi potential, which is expressed as [64]:

$$\varepsilon = RT \ln\left(1 + \frac{1}{C_e}\right) \tag{10}$$

where R (J/mol K) is the gas constant, T (K) is the temperature, and C_e (mg/L) is the equilibrium TAN concentration.

β depends on the average adsorption energy of the adsorbate per mole of adsorbent when the adsorbate molecules in the solution are transferred to the surface of the adsorbent from infinite distance. The value of β can be obtained from the slope of the D–R plot ($\ln(q_e)$ vs. ε^2). Finally, the adsorption energy can be reached by the following equation.

$$E = \frac{1}{\sqrt{2\beta}} \tag{11}$$

The adsorption processes with E values ranging from 1 to 8 kJ/mol are typically considered as physisorption whereas

9 to 16 kJ/mol are classified as chemisorption [67]. The *E* value determined for this study by the D–R method was 0.5 kJ/mol, which is a weak interaction.

3.4. Thermodynamic

A thermodynamic approach was used to analyze the temperature dependence of adsorption mechanisms in more detail. As the temperature increased from 7°C to 42°C, the solid phase concentration decreases from 22.7 to 20.4 mg/g and the removal percentage drops from 47% to 44%. This indicates that the process was exothermic.

The thermodynamic parameters including enthalpy changes (ΔH) and entropy changes (ΔS) were determined using the results at different temperatures of 7°C, 24°C, and 42°C using the van't Hoff equation shown below [62,67].

$$\log K_d = \frac{\Delta S}{2.303R} - \frac{\Delta H}{2.303RT} \tag{12}$$

where T is the temperature in Kelvin; R is the universal gas constant (8.314 J/mol K); ΔH (J/mol) is the enthalpy change; ΔS (J/mol K) is the entropy change; K_d is the equilibrium constant determined as [62,68,69]:

$$K_d = 1000\frac{q_e}{C_e} \tag{13}$$

where q_e (mg/g) and C_e (mg/L) are equilibrium solid phase concentration and equilibrium TAN concentration, respectively.

Thermodynamic parameters are summarized in Table 2. The negative value of ΔH (–2.35 kJ/mol) confirms that the adsorption process is exothermic, which is in agreement with the results above [70]. Additionally, some studies have reported that a ΔH value lower than 8 kJ/mol could be an indication of an ion exchange process [22,26]. This suggests that the adsorption process consisted of ion exchange of NH_4^+ by Na^+ on GO-Na [71]; because at neutral pH and room temperature, TAN in solution is mainly ammonium cations. The observation of the process being dominated by ion exchange is in agreement with the results obtained from the D–R isotherm.

The positive value of ΔS (0.048 kJ/mol K) can be explained by the increasing randomness at the solid–liquid interface during the exothermic adsorption of TAN on the adsorbent surface which confirms the favorability of the process [26]. The results obtained and presented for ΔH and ΔS in this study (Table 2) are in agreement with results by various previous research (Rat-Valdambrini et al. [26]; Saltalı et al. [22]; Boopathy et al. [72]; and Vassileva and Voikova [18]). Who also reported the low values of ΔH and ΔS for ammonium uptake by various adsorbent including zeolites and coconut shell-activated carbon indicates that the interaction between NH_4^+ and the active site on the surface of adsorbent is weak. Furthermore, the process with ΔG ranging from –20 to 0 is generally considered as a physisorption process and the one with a ΔG ranging from –400 to –80 as a chemisorption process. The negative value of ΔG demonstrates the spontaneity of a reaction, and the value obtained is consistent with the weak interaction nature of the process [73,74].

Table 2
Thermodynamic parameters of TAN adsorption onto GO-Na. Conditions: pH = 7, C_0 = 50 mg/L, and dose = 1 g GO-Na/L

T (°K)	ΔH (kJ/mol)	ΔS (kJ/mol K)	ΔG (kJ/mol)
280			–15.8
297	–2.346	0.048	–16.62
315			–17.48

3.5. Adsorption kinetics

Four consecutive kinetic steps are usually considered in a sorption process, namely transport in the bulk solution (particle diffusion), diffusion across the film surrounding the sorbent particles (film diffusion), intra-particle mass transfer within the particle [75] (intra-particle diffusion), and finally sorption and desorption on the solid surface considered as a kind of chemical reaction [76]. The rate of adsorption is controlled by the slowest step which can usually be classified into two main categories. First, a diffusion-controlled process and second, the process controlled by the chemical reaction between adsorbate molecules in the solution and the molecules on the surface of the adsorbent [77]. To investigate if the diffusion steps control the adsorption kinetics, the intra-particle diffusion model was utilized to describe the effects of diffusion on the adsorption mechanism. Moreover, to study the role of the chemical reaction, the adsorption data were fitted using Elovich's reaction model. The equations are expressed as follows:

Intra-particle diffusion:

$$q_t = k_{\mathrm{id}} t^{\frac{1}{2}} + \mathrm{C} \tag{14}$$

where q_t (mg/g) is the solid phase concentration at time t; k_{id} (mg/g $\mathrm{min}^{½}$) is the intra-particle rate constant; C (mg/g) represents the thickness of boundary layer and it can be obtained from the interception of the plot of q_t vs. $t^{½}$ [78]. If C is equal to zero, it can be interpreted that the intra-particle diffusion is the only controlling factor in the adsorption process. In this study, the nonzero value of C (19.03 mg/g) suggests that in this process more than one factor can play a role in the rate-controlling of the whole process [75].

Elovich's reaction:

$$q_t = \frac{1}{\beta}\ln(\alpha\beta) + \frac{1}{\beta}\ln(t) \tag{15}$$

where α (mg/g min) and β (g/mg) are the Elovich's constant which represents the initial adsorption rate and the desorption coefficient, respectively [79,80].

To compare these two models, it is essential to have dimensionless parameters that better quantify the likelihood of TAN adsorption on a particular adsorbent. In this regard, intra-particle and Elovich equations were modified. The dimensionless equations were obtained according to the method of Wu et al. [79].

Dimensionless intra-particle diffusion:

$$\frac{q_t}{q_{\text{ref}}} = 1 - R_{\text{id}}\left(1 - \left(\frac{t}{t_{\text{ref}}}\right)^{\frac{1}{2}}\right) \tag{16}$$

Dimensionless Elovich equation:

$$\frac{q_t}{q_{\text{ref}}} = \frac{1}{\beta q_{\text{ref}}}\ln\left(\frac{t}{t_{\text{ref}}}\right) + 1 \tag{17}$$

where t_{ref} is defined as the longest time in the adsorption process and subsequently q_{ref} is the solid phase concentration at time $t = t_{\text{ref}}$. R_{id} is a dimensionless starting adsorption factor of the intra-particle diffusion model defined as $R_{\text{id}} = k_{\text{id}}\frac{t_{\text{ref}}^{\frac{1}{2}}}{q_{\text{ref}}}$.

Fig. 7 illustrates the best fit of experimental data using the dimensionless form of the intra-particle and Elovich equations. As it is depicted in Fig. 7, the Elovich model contains two linear portions indicating the adsorption of ammonium cations occurs in two stages. The first portion, with a steep slope, can be explained by the instant diffusion of ammonium cations through the solution and exchange with sodium-containing ligands on the surface of GO (film diffusion). There are three theories to explain the second portion: (1) after a few minutes, the diffusion term decreases because many ammonium cations are already adsorbed to the surface of the adsorbent decreasing the concentration of ammonium ions in solution at the vicinity of the adsorbent, (2) there are fewer sodium cations on the surface of the adsorbent to be exchanged by ammonium, because some of them are already exchanged [53,78], and (3) the reactivity of ammonium with the adsorbent transitions from ion exchange to reaction with the oxygen of the GO backbone which leads to the saturation of the surface by chemisorbed species [71,81].

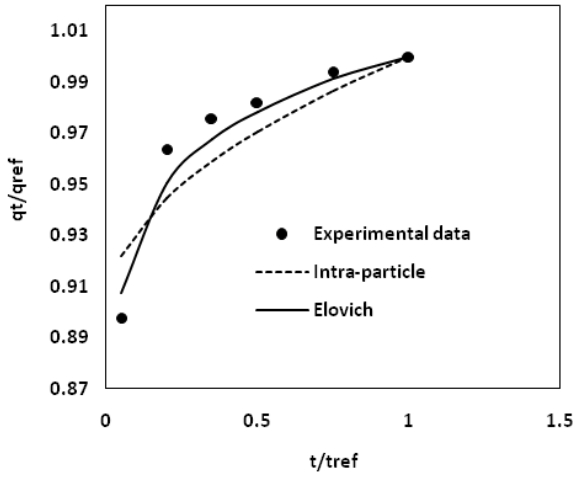

Fig. 7. Fitting of experimental data with dimensionless form of intra-particle and Elovich equation. Conditions: at room temperature, pH = 7, C_0 = 50 mg/L, and dose = 1 g GO-Na/L

The Elovich equation is usually used to determine whether the chemical reaction on the heterogeneous surface of adsorbent is the rate-limiting step. A better fit of Elovich model (R^2 = 0.960) compared to intra-particle diffusion (R^2 = 0.838) suggests that chemical reaction is rate-limiting for this process.

A kinetic analysis was used to determine the optimum operating time to reach equilibrium for the full-scale batch adsorption process [19]. The kinetic parameters specify the effect of contact time on the removal percentage and solid-phase concentration of adsorbent. The adsorption mechanism of TAN on GO-Na has been examined by pseudo-first-order and pseudo-second-order models [34,53,80,82–84] which were defined as follow:

Pseudo-first-order:

$$\ln\left(q_e - q_t\right) = -k_1 t + \ln q_e \tag{18}$$

Pseudo-second-order:

$$\frac{t}{q_t} = \frac{1}{k_2 q_e^2} + \frac{t}{q_e} \tag{19}$$

where q_t, q_e (mg/g) are the solid phase concentration at time t and equilibrium, respectively. k_1 (min^{-1}) and k_2 (g/mg min) are the rate constant for the pseudo-first and second-order-model, respectively.

The experimental data were plotted according to pseudo-first and second-order models shown in Fig. 8 and parameters for these models are calculated and summarized in Table 3. As could be expected by the typical adsorption behavior of exchange materials [33,40,75], the pseudo-second-order model fits with a much higher regression correlation (0.999) indicating that this is the best fitting model for the process. Further strong evidence that the experimental adsorption is best described by pseudo-second-order is the theoretical solid-phase concentration (q_e) calculated according to the pseudo-second-order model matches the experimentally determined value. The initial adsorption rate V_0 (mg/g min) for pseudo-second-order is equal to $k_2 q_e^2$. The high value of V_0 (118 mg/g min) verifies the fact that the adsorption process is very fast. Also, the batch adsorption experiments revealed that the final equilibrium condition is reached within a few minutes, making the process appealing from a practical point of view [85]. The fast kinetics would also allow a smaller and more economical flow reactor.

The pseudo-second-order model is typically indicative of chemical sorption rate-controlling processes [86]. The chemical sorption process includes valence forces created between adsorbent and adsorbate by sharing or exchanging electrons [40]. The pseudo-second-order model assumes that the rate-controlling step of the TAN adsorption process is a consequence of chemical sorption and more than one-step may be involved in sorption processes [80].

There is consistency between the Elovich model and the determined pseudo-second-order kinetics. That is, the low average value of the adsorption energy suggests a complex adsorption behavior where there is chemical interaction between ammonium ions and different absorption sites in GO-Na. Binding to each site may have a slightly different rate constant, leading to the overall pseudo-second-order

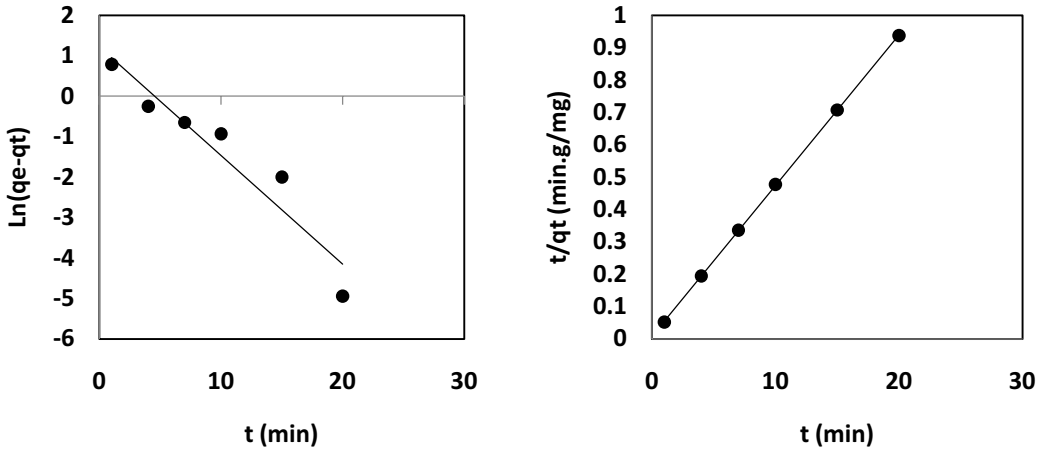

Fig. 8. Fitting of experimental data with (a) pseudo-first-order and (b) pseudo-second-order model. Conditions: at room temperature, pH = 7, C_0 = 50 mg TAN/L, and dose = 1 g GO-Na/ L.

Table 3
Kinetic parameters of TAN adsorption on GO-Na

Kinetic model	q_e (mg/g)	k	R^2
Pseudo-first-order	3.39	0.27 (min^{-1})	0.911
Pseudo-second-order	21.5	0.25 (min mg/g)	0.999

behavior, yet the binding shows a weak interaction expected for ion-exchange. This fact makes the adsorbent more promising because its regeneration will be more effective and practical.

3.6. Regeneration of adsorbent

As the range of adsorption energy and the results obtained from thermodynamic studies confirmed the adsorption process is due to weak interactions, the ion exchange of ammonium and sodium cations can be expected to be reversible. Therefore, sodium chloride, a nontoxic and inexpensive salt in industry, is used for regeneration of the adsorbent to make this process more economical and environmentally friendly. The performance of reused adsorbent was studied for several regeneration cycles. Fig. 9 shows the removal percentage and incremental solid-phase concentration of regenerated GO-Na for 3 cycles. Fig. 9 shows 5% and 2 mg/g loss in removal percentage and incremental solid phase concentration, respectively, in each cycle. It can be concluded that GO-Na can remain effective after several cycles.

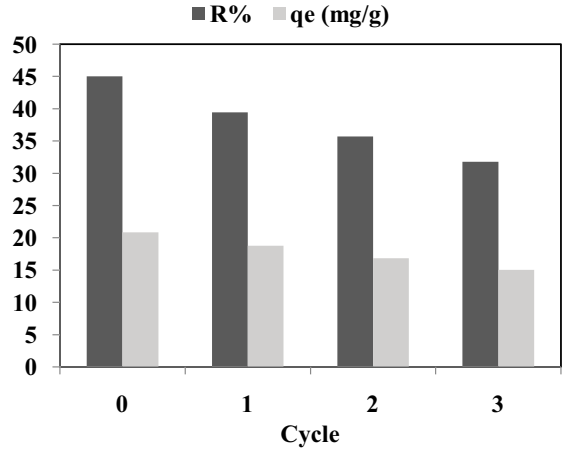

Fig. 9. Regeneration cycle of GO-Na for TAN removal. Conditions: C_0 = 50 mg/L, dose = 1 g GO-Na/L, neutral pH, and room temperature.

4. Conclusion

Experimental results indicate that GO-Na is an efficient adsorbent to remove TAN from aqueous solution. The Langmuir model provided the best prediction for the TAN removal process with a maximum adsorption capacity of 32 mg/g. The small values of the adsorption energy, enthalpy, entropy, and Gibb's free energy suggest that the adsorption mainly consists of ion exchange processes with weak interaction between adsorbate and adsorbent. A kinetic study shows that this process is very fast which makes GO-Na a promising adsorbent from the practical points of view. This adsorption process is best described by the pseudo-second-order model indicates that chemisorption is the rate-controlling step. The mechanism of adsorbent is well described by the Elovich model suggesting that the rate-controlling step in this process is a chemical reaction, which occurs with a slower rate rather than ion exchange of NH_4^+ with Na^+ on the surface of the adsorbent. Thermodynamic studies indicate that adsorption of TAN on GO-Na is exothermic with increasing randomness at the solid-liquid interface. The negative values of Gibb's free energy indicate that this adsorption process is spontaneous. The weak interactions between adsorbate and adsorbent efficiently facilitate the regeneration of GO-Na.

Acknowledgments

The authors are grateful to the Center for Catalysis Research and Innovation at the University of Ottawa for access to the facilities. Funding from the Natural Sciences and Engineering Research Council of Canada is acknowledged.

References

[1] M. Henze, P. Harremoes, J. la Cour Jansen, E. Arvin, Wastewater Treatment: Biological and Chemical Processes, 3rd ed., Springer, Berlin, Germany, 2001.

[2] X.-e. Yang, X. Wu, H.-l. Hao, Z.-l. He, Mechanisms and assessment of water eutrophication, J. Zhejiang Univ. Sci. B, 9 (2008) 197–209.

[3] J. Heisler, P.M. Glibert, J.M. Burkholder, D.M. Anderson, W. Cochlan, W.C. Dennison, C. Gobler, Q. Dortch, C. Heil, E. Humphries, A. Lewitus, R. Magnien, H. Marshall, K. Sellner, D. Stockwell, D. Stoecker, M. Suddleson, Eutrophication and harmful algal blooms: a scientific consensus, Harmful Algae, 8 (2008) 3–13.

[4] US EPA Office of Water 4304T, Aquatic Life Ambient Water Quality Criteria for Ammonia - Freshwater, EPA 822-R-18-002, United States Environmental Protection Agency, Office of Science and Technology, Washington, D.C., USA, 2013.

[5] J. Netting, North Carolina reflects on ammonia controls, Nature, 406 (2000) 928.

[6] C.-y. Zou, S.-q. Liu, Z.M. Shen, Y. Zhang, N.-s. Jiang, W.-c. Ji, Efficient removal of ammonia with a novel graphene-supported $BiFeO_3$ as a reusable photocatalyst under visible light, Chin. J. Catal., 38 (2017) 20–28.

[7] K. Emerson, R.C. Russo, R.E. Lund, R.V. Thurston, Aqueous ammonia equilibrium calculations: effect of pH and temperature, J. Fish. Board Canada, 32 (1975) 2379–2383.

[8] S.-j. Zhang, Y.-z. Peng, S.-y. Wang, S.-w. Zheng, G. Jin, Organic matter and concentrated nitrogen removal by shortcut nitrification and denitrification from mature municipal landfill leachate, J. Environ. Sci., 19 (2007) 647–651.

[9] A.C. Silva, M. Dezotti, G.L. Sant'Anna Jr., Treatment and detoxification of a sanitary landfill leachate, Chemosphere, 55 (2004) 207–214.

[10] X.Z. Li, Q.L. Zhao, X.D. Hao, Ammonium removal from landfill leachate by chemical precipitation, Waste Manage., 19 (1999) 409–415.

[11] S. Dong, M. Sartaj, Statistical analysis and optimization of ammonia removal from landfill leachate by sequential microwave/aeration process using factorial design and response surface methodology, J. Environ. Chem. Eng., 4 (2016) 100–108.

[12] Q. Du, S.J. Liu, Z.H. Cao, Y.Q. Wang, Ammonia removal from aqueous solution using natural Chinese clinoptilolite, Sep. Purif. Technol., 44 (2005) 229–234.

[13] Y.-F. Wang, F. Lin, W.-Q. Pang, Ammonium exchange in aqueous solution using Chinese natural clinoptilolite and modified zeolite, J. Hazard. Mater., 142 (2007) 160–164.

[14] M. Sprynskyy, M. Lebedynets, R. Zbytniewski, J. Namieśnik, B. Buszewski, Ammonium removal from aqueous solution by natural zeolite, Transcarpathian mordenite, kinetics, equilibrium and column tests, Sep. Purif. Technol., 46 (2005) 155–160.

[15] M. Zhang, H.Y. Zhang, D. Xu, L. Han, D.X. Niu, L. Zhang, W. Wu, B.H. Tian, Ammonium removal from aqueous solution by zeolites synthesized from low-calcium and high-calcium fly ashes, Desalination, 277 (2011) 46–53.

[16] H.M. Huang, X.M. Xiao, B. Yan, L.P. Yang, Ammonium removal from aqueous solutions by using natural Chinese (Chende) zeolite as adsorbent, J. Hazard. Mater., 175 (2010) 247–252.

[17] L.C. Lei, X.J. Li, X.W. Zhang, Ammonium removal from aqueous solutions using microwave-treated natural Chinese zeolite, Sep. Purif. Technol., 58 (2008) 359–366.

[18] P. Vassileva, D. Voikova, Investigation on natural and pretreated Bulgarian clinoptilolite for ammonium ions removal from aqueous solutions, J. Hazard. Mater., 170 (2009) 948–953.

[19] A.M. Yusof, L.K. Keat, Z. Ibrahim, Z.A. Majid, N.A. Nizam, Kinetic and equilibrium studies of the removal of ammonium ions from aqueous solution by rice husk ash-synthesized zeolite Y and powdered and granulated forms of mordenite, J. Hazard. Mater., 174 (2010) 380–385.

[20] M. Zhang, H.Y. Zhang, D. Xu, L. Han, D.X. Niu, B.H. Tian, J. Zhang, L.Y. Zhang, W.S. Wu, Removal of ammonium from aqueous solutions using zeolite synthesized from fly ash by a fusion method, Desalination, 271 (2011) 111–121.

[21] D. Karadag, Y. Koc, M. Turan, B. Armagan, Removal of ammonium ion from aqueous solution using natural Turkish clinoptilolite, J. Hazard. Mater., 136 (2006) 604–609.

[22] K. Saltalı, A. Sarı, M. Aydın, Removal of ammonium ion from aqueous solution by natural Turkish (Yıldızeli) zeolite for environmental quality, J. Hazard. Mater., 141 (2007) 258–263.

[23] J.Y. Huang, N.R. Kankanamge, C. Chow, D.T. Welsh, T.L. Li, P.R. Teasdale, Removing ammonium from water and wastewater using cost-effective adsorbents: a review, J. Environ. Sci., 63 (2018) 174–197.

[24] N. Zhao, H. Wang, Z. He, Q. Yan, Ammonia removal and recovery from diluted forward osmosis draw solution by using a tubular microbial desalination cell, Environ. Sci. Water Res. Technol., 5 (2019) 224–230.

[25] R.B.B. Kammoe, S. Hamoudi, Investigation of ammonium ion removal from aqueous solutions using arene- and propylsulfonic acid functionalized mesoporous silica adsorbents, J. Environ. Qual., 43 (2014) 1032–1042.

[26] M. Rat-Valdambrini, K. Belkacemi, S. Hamoudi, Removal of ammonium cations from aqueous solution using arene-sulphonic acid functionalised SBA-15 as adsorbent, Can. J. Chem. Eng., 90 (2012) 18–25.

[27] Y. Ding, M. Sartaj, Optimization of ammonia removal by ion-exchange resin using response surface methodology, Int. J. Environ. Sci. Technol., 13 (2016) 985–994.

[28] T.C. Jorgensen, L.R. Weatherley, Ammonia removal from wastewater by ion exchange in the presence of organic contaminants, Water Res., 37 (2003) 1723–1728.

[29] Y.H. Ding, M. Sartaj, Statistical analysis and optimization of ammonia removal from aqueous solution by zeolite using factorial design and response surface methodology, J. Environ. Chem. Eng., 3 (2015) 807–814.

[30] Y. Ding, Statistical Analysis and Optimization of Ammonia Removal from Aqueous Solution by Zeolite and Ion-exchange Resin, Université d'Ottawa/uOttawa, 2015.

[31] Y. Jiang, P. Biswas, J.D. Fortner, A review of recent developments in graphene-enabled membranes for water treatment, Environ. Sci. Water Res. Technol., 2 (2016) 915–922.

[32] Y. Zhu, S. Murali, W. Cai, X. Li, J.W. Suk, J.R. Potts, R.S. Ruoff, Graphene and graphene oxide: synthesis, properties, and applications, Adv. Mater., 22 (2010) 3906–3924.

[33] Y.H. Li, Q.J. Du, T.H. Liu, X.J. Peng, J.J. Wang, J.K. Sun, Y.H. Wang, S.L. Wu, Z.H. Wang, Y.Z. Xia, L.H. Xia, Comparative study of methylene blue dye adsorption onto activated carbon, graphene oxide, and carbon nanotubes, Chem. Eng. Res. Des., 91 (2013) 361–368.

[34] C.P. Li, M. She, X.D. She, J. Dai, L.X. Kong, Functionalization of polyvinyl alcohol hydrogels with graphene oxide for potential dye removal, J. Appl. Polym. Sci., 131 (2014) 39872.

[35] N.A. Travlou, G.Z. Kyzas, N.K. Lazaridis, E.A. Deliyanni, Graphite oxide/chitosan composite for reactive dye removal, Chem. Eng. J., 217 (2013) 256–265.

[36] H.Y. Guo, T.F. Jiao, Q.R. Zhang, W.F. Guo, Q.M. Peng, X.H. Yan, Preparation of graphene oxide-based hydrogels as efficient dye adsorbents for wastewater treatment, Nanoscale Res. Lett., 10 (2015) 272.

[37] L.L. Fan, C.N. Luo, M. Sun, H.M. Qiu, X.J. Li, Synthesis of magnetic β-cyclodextrin–chitosan/graphene oxide as nano-adsorbent and its application in dye adsorption and removal, Colloids Surf., B, 103 (2013) 601–607.

[38] G.Z. Kyzas, A. Koltsakidou, S.G. Nanaki, D.N. Bikiaris, D.A. Lambropoulou, Removal of beta-blockers from aqueous media by adsorption onto graphene oxide, Sci. Total Environ., 537 (2015) 411–420.

[39] A. Carmalin Sophia, E.C. Lima, N. Allaudeen, S. Rajan, Application of graphene based materials for adsorption of pharmaceutical traces from water and wastewater-a review, Desal. Wat. Treat., 57 (2016) 27573–27586.

[40] X. Mi, G.B. Huang, W.S. Xie, W. Wang, Y. Liu, J.P. Gao, Preparation of graphene oxide aerogel and its adsorption for Cu^{2+} ions, Carbon, 50 (2012) 4856–4864.

[41] G.X. Zhao, J.X. Li, X.M. Ren, C.L. Chen, X.K. Wang, Few-layered graphene oxide nanosheets as superior sorbents for heavy metal ion pollution management, Environ. Sci. Technol., 45 (2011) 10454–10462.
[42] Y.-C. Lee, J.-W. Yang, Self-assembled flower-like TiO_2 on exfoliated graphite oxide for heavy metal removal, J. Ind. Eng. Chem., 18 (2012) 1178–1185.
[43] F. Zhou, X.Z. Feng, J.G. Yu, X.Y. Jiang, High performance of 3D porous graphene/lignin/sodium alginate composite for adsorption of Cd(II) and Pb(II), Environ. Sci. Pollut. Res., 25 (2018) 1–11.
[44] X.Z. Yang, T.Z. Zhou, B. Ren, A. Hursthouse, Y.Z. Zhang, Removal of Mn (II) by sodium alginate/graphene oxide composite double-network hydrogel beads from aqueous solutions, Sci. Rep., 8 (2018) 10717.
[45] M. Seredych, J.A. Rossin, T.J. Bandosz, Changes in graphite oxide texture and chemistry upon oxidation and reduction and their effect on adsorption of ammonia, Carbon, 49 (2011) 4392–4402.
[46] C. Petit, T.J. Bandosz, Enhanced adsorption of ammonia on metal-organic framework/graphite oxide composites: analysis of surface interactions, Adv. Funct. Mater., 20 (2010) 111–118.
[47] C. Petit, T.J. Bandosz, Synthesis, characterization, and ammonia adsorption properties of mesoporous metal–organic framework (MIL(Fe))–graphite oxide composites: exploring the limits of materials fabrication, Adv. Funct. Mater., 21 (2011) 2108–2117.
[48] S.S. Chen, W.W. Cai, D. Chen, Y.J. Ren, X.S. Li, Y.W. Zhu, J.Y. Kang, R.S. Ruoff, Adsorption/desorption and electrically controlled flipping of ammonia molecules on graphene, New J. Phys., 12 (2010) 125011.
[49] N.M. Huang, H.N. Lim, C.H. Chia, M.A. Yarmo, M.R. Muhamad, Simple room-temperature preparation of high-yield large-area graphene oxide, Int. J. Nanomed., 6 (2011) 3443.
[50] S. Verma, R.K. Dutta, A facile method of synthesizing ammonia modified graphene oxide for efficient removal of uranyl ions from aqueous medium, RSC Adv., 5 (2015) 77192–77203.
[51] M.P. Kumar, T. Kesavan, G. Kalita, P. Ragupathy, T.N. Narayanan, D.K. Pattanayak, On the large capacitance of nitrogen doped graphene derived by a facile route, RSC Adv., 4 (2014) 38689–38697.
[52] B. Dehghanzad, M.K.R. Aghjeh, O. Rafeie, A. Tavakoli, A.J. Oskooie, Synthesis and characterization of graphene and functionalized graphene via chemical and thermal treatment methods, RSC Adv., 6 (2016) 3578–3585.
[53] A.R. Badiei, A. Mirahsani, A. Shahbazi, H. Younesi, M. Alizadeh, Adsorptive removal of toxic dye from aqueous solution and real industrial effluent by tris(2-aminoethyl)amine functionalized nanoporous silica, Environ. Prog. Sustainable Energy, 33 (2014) 1242–1250.
[54] F. Gimbert, N. Morin-Crini, F. Renault, P.-M. Badot, G. Crini, Adsorption isotherm models for dye removal by cationized starch-based material in a single component system: error analysis, J. Hazard. Mater., 157 (2008) 34–46.
[55] I.D. Mall, V.C. Srivastava, N.K. Agarwal, Removal of Orange-G and Methyl Violet dyes by adsorption onto bagasse fly ash—kinetic study and equilibrium isotherm analyses, Dyes Pigm., 69 (2006) 210–223.
[56] R. Malekian, J. Abedi-Koupai, S.S. Eslamian, S.F. Mousavi, K.C. Abbaspour, M. Afyuni, Ion-exchange process for ammonium removal and release using natural Iranian zeolite, Appl. Clay Sci., 51 (2011) 323–329.
[57] V.K. Jha, S. Hayashi, Modification on natural clinoptilolite zeolite for its NH_4^+ retention capacity, J. Hazard. Mater., 169 (2009) 29–35.
[58] A. Alshameri, C.J. Yan, Y. Al-Ani, A.S. Dawood, A. Ibrahim, C.Y. Zhou, H.Q. Wang, An investigation into the adsorption removal of ammonium by salt activated Chinese (Hulaodu) natural zeolite: kinetics, isotherms, and thermodynamics, J. Taiwan Inst. Chem. Eng., 45 (2014) 554–564.
[59] E. Marañón, M. Ulmanu, Y. Fernández, I. Anger, L. Castrillón, Removal of ammonium from aqueous solutions with volcanic tuff, J. Hazard. Mater., 137 (2006) 1402–1409.
[60] M. Sica, A. Duta, C. Teodosiu, C. Draghici, Thermodynamic and kinetic study on ammonium removal from a synthetic water solution using ion exchange resin, Clean Technol. Environ. Policy, 16 (2014) 351–359.
[61] A.A. Halim, H.A. Aziz, M.A.M. Johari, K.S. Ariffin, Comparison study of ammonia and COD adsorption on zeolite, activated carbon and composite materials in landfill leachate treatment, Desalination, 262 (2010) 31–35.
[62] S. Maji, A. Ghosh, K. Gupta, A. Ghosh, U. Ghorai, A. Santra, P. Sasikumar, U.C. Ghosh, Efficiency evaluation of arsenic(III) adsorption of novel graphene oxide@iron-aluminium oxide composite for the contaminated water purification, Sep. Purif. Technol., 197 (2018) 388–400.
[63] M.J.K. Bashir, H.A. Aziz, M.S. Yusoff, M.N. Adlan, Application of response surface methodology (RSM) for optimization of ammoniacal nitrogen removal from semi-aerobic landfill leachate using ion exchange resin, Desalination, 254 (2010) 154–161.
[64] A.A. Inyinbor, F.A. Adekola, G.A. Olatunji, Kinetics, isotherms and thermodynamic modeling of liquid phase adsorption of Rhodamine B dye onto *Raphia hookerie* fruit epicarp, Water Resour. Ind., 15 (2016) 14–27.
[65] N. Ayawei, A.N. Ebelegi, D. Wankasi, Modelling and interpretation of adsorption isotherms, J. Chem., 2017 (2017) 11 pages, https://doi.org/10.1155/2017/3039817.
[66] Y.S. Ho, C.T. Huang, H.W. Huang, Equilibrium sorption isotherm for metal ions on tree fern, Process Biochem., 37 (2002) 1421–1430.
[67] V.J. Inglezakis, A.A. Zorpas, Heat of adsorption, adsorption energy and activation energy in adsorption and ion exchange systems, Desal. Wat. Treat., 39 (2012) 149–157.
[68] S. Chowdhury, R. Mishra, P. Saha, P. Kushwaha, Adsorption thermodynamics, kinetics and isosteric heat of adsorption of malachite green onto chemically modified rice husk, Desalination, 265 (2011) 159–168.
[69] Y. Liu, Is the free energy change of adsorption correctly calculated?, J. Chem. Eng. Data, 54 (2009) 1981–1985.
[70] G. Vijayakumar, R. Tamilarasan, M. Dharmendirakumar, Adsorption, kinetic, equilibrium and thermodynamic studies on the removal of basic dye Rhodamine-B from aqueous solution by the use of natural adsorbent perlite, J. Mater. Environ. Sci., 3 (2012) 157–170.
[71] S.B. Tang, Z.X. Cao, Adsorption and dissociation of ammonia on graphene oxides: a first-principles study, J. Phys. Chem. C, 116 (2012) 8778–8791.
[72] R. Boopathy, S. Karthikeyan, A.B. Mandal, G. Sekaran, Adsorption of ammonium ion by coconut shell-activated carbon from aqueous solution: kinetic, isotherm, and thermodynamic studies, Environ. Sci. Pollut. Res., 20 (2013) 533–542.
[73] C.-H. Huang, K.-P. Chang, H.-D. Ou, Y.-C. Chiang, C.-F. Wang, Adsorption of cationic dyes onto mesoporous silica, Microporous Mesoporous Mater., 141 (2011) 102–109.
[74] Y. Wimalasiri, M. Mossad, L. Zou, Thermodynamics and kinetics of adsorption of ammonium ions by graphene laminate electrodes in capacitive deionization, Desalination, 357 (2015) 178–188.
[75] G.K. Ramesha, A.V. Kumara, H.B. Muralidhara, S. Sampath, Graphene and graphene oxide as effective adsorbents toward anionic and cationic dyes, J. Colloid Interface Sci., 361 (2011) 270–277.
[76] W. Rudzinski, W. Plazinski, Theoretical description of the kinetics of solute adsorption at heterogeneous solid/solution interfaces: on the possibility of distinguishing between the diffusional and the surface reaction kinetics models, Appl. Surf. Sci., 253 (2007) 5827–5840.
[77] J.-P. Simonin, On the comparison of pseudo-first order and pseudo-second order rate laws in the modeling of adsorption kinetics, Chem. Eng. J., 300 (2016) 254–263.
[78] E. Repo, J.K. Warchol, T.A. Kurniawan, M.E.T. Sillanpää, Adsorption of Co(II) and Ni(II) by EDTA- and/or DTPA-modified chitosan: kinetic and equilibrium modeling, Chem. Eng. J., 161 (2010) 73–82.
[79] F.-C. Wu, R.-L. Tseng, R.-S. Juang, Characteristics of Elovich equation used for the analysis of adsorption kinetics in dye-chitosan systems, Chem. Eng. J., 150 (2009) 366–373.

[80] H. Wang, X.Z. Yuan, Y. Wu, H.J. Huang, G.M. Zeng, Y. Liu, X.L. Wang, N.B. Lin, Y. Qi, Adsorption characteristics and behaviors of graphene oxide for Zn(II) removal from aqueous solution, Appl. Surf. Sci., 279 (2013) 432–440.
[81] E.C. Mattson, K. Pande, M. Unger, S.M. Cui, G.H. Lu, M. Gajdardziska-Josifovska, M. Weinert, J.H. Chen, C.J. Hirschmugl, Exploring adsorption and reactivity of NH_3 on reduced graphene oxide, J. Phys. Chem. C, 117 (2013) 10698–10707.
[82] S.B. Wang, H.T. Li, L.Y. Xu, Application of zeolite MCM-22 for basic dye removal from wastewater, J. Colloid Interface Sci., 295 (2006) 71–78.
[83] L. Largitte, R. Pasquier, A review of the kinetics adsorption models and their application to the adsorption of lead by an activated carbon, Chem. Eng. Res. Des., 109 (2016) 495–504.
[84] Y.S. Ho, J.C.Y. Ng, G. McKay, Kinetics of pollutant sorption by biosorbents, Sep. Purif. Methods, 29 (2000) 189–232.
[85] S. Bai, X.P. Shen, X. Zhong, Y. Liu, G.X. Zhu, X. Xu, K.M. Chen, One-pot solvothermal preparation of magnetic reduced graphene oxide-ferrite hybrids for organic dye removal, Carbon, 50 (2012) 2337–2346.
[86] G.Z. Kyzas, E.A. Deliyanni, K.A. Matis, Graphene oxide and its application as an adsorbent for wastewater treatment, J. Chem. Technol. Biotechnol., 89 (2014) 196–205.